Adaptive Global Sliding-Mode Control for Dynamic Systems Using Double Hidden Layer Recurrent Neural Network Structure

Yundi Chu, Juntao Fei, *Senior Member, IEEE*, and Shixi Hou

***Abstract*— In this paper, a full-regulated neural network (NN) with a double hidden layer recurrent neural network (DHLRNN) structure is designed, and an adaptive global sliding-mode controller based on the DHLRNN is proposed for a class of dynamic systems. Theoretical guidance and adaptive adjustment mechanism are established to set up the base width and central vector of the Gaussian function in the DHLRNN structure, where six sets of parameters can be adaptively stabilized to their best values according to different inputs. The new DHLRNN can improve the accuracy and generalization ability of the network, reduce the number of network weights, and accelerate the network training speed due to the strong fitting and presentation ability of two-layer activation functions compared with a general NN with a single hidden layer. Since the neurons of input layer can receive signals which come back from the neurons of output layer in the output feedback neural structure, it can possess associative memory and rapid system convergence, achieving better approximation and superior dynamic capability. Simulation and experiment on an active power filter are carried out to indicate the excellent static and dynamic performances of the proposed DHLRNN-based adaptive global sliding-mode controller, verifying its best approximation performance and the most stable internal state compared with other schemes.**

***Index Terms*— Double hidden layer recurrent neural network (DHLRNN), global sliding-mode control (GSMC), single hidden layer neural network (SHLNN), single hidden layer recurrent neural network (SHLRNN).**

I. Introduction

DYNAMIC systems always have unknown parameter variations and external disturbances which seem to be difficult to deal with using traditional control schemes. Sliding-mode controller, which was employed in the position and speed control of nonlinear systems recently [1]–[5], is insensitive to parameter variations and external disturbances. A novel optimal guaranteed cost sliding-mode control was designed for constrained-input nonlinear systems with matched and unmatched disturbances in [1]. Kühne *et al.* [2] derived a two-input sliding-mode controller, which controls both phase difference and frequency of the traveling wave without implementing a signum function. Ghahderijani *et al.* [3] presented a sliding-mode control scheme to provide high robustness to external disturbances and transient response during large and abrupt load changes. Song *et al.* [4] introduced a novel continuous controller based on a full-order terminal sliding-mode method. Xiong *et al.* [5] developed a fractional order sliding-mode control strategy for a grid-connected doubly fed induction generator.

However, the application of pure conventional sliding-mode control is limited because it cannot realize global robustness during the whole system process. For this, a global sliding-mode controller is introduced, which can solve the shortcoming of the traditional one [6]–[10]. Chu and Fei [6] was concerned with an adaptive dynamic global sliding-mode controller based on a proportional integral derivative sliding surface using a radial basis function neural network (NN) for a three-phase active power filter (APF) to obtain global robustness. The procedure for a global sliding-mode observer design for nonlinear locally Lipschitz systems with a high relative degree was proposed in [7]. Hu *et al.* [8] focused on a novel global sliding-mode control (GSMC) based on a hyperbolic tangent function for matrix rectifiers. Liu *et al.* [9] learnt the stabilization problem for a class of nonlinear systems using a GSMC approach. Mobayen and Baleanu [10] presented a novel GSMC technique for the stabilization of a class of uncertain and nonlinear dynamic systems to guarantee the asymptotic stabilization.

Although global sliding-mode controller can achieve favorable tracking performance in the presence of system uncertainties and external disturbances, it cannot be easily implemented, because it is based on a good understanding of a model structure. The feedforward NN has been widely applied in identification and control for its strong capacity to approximate any unknown smooth functions of dynamic systems [11]–[20]. Chien *et al.* [11] studied the tracking and almost disturbance decoupling problem of nonlinear

Manuscript received May 24, 2018; revised December 26, 2018, April 3, 2019, and April 24, 2019; accepted May 24, 2019. This work was supported in part by the National Science Foundation of China under Grant 61873085, in part by the Natural Science Foundation of Jiangsu Province under Grant BK20171198 and Grant BK20170303, in part by the University Graduate Research and Innovation Projects of Jiangsu Province under Grant 2018B676X14, and in part by the Fundamental Research Funds for the Central Universities under Grant 2017B07011, Grant 2017B20014, and Grant 2017B03014. *(Corresponding author: Juntao Fei.)*

Y. Chu and J. Fei are with the College of Energy and Electrical Engineering, Hohai University, Nanjing 210098, China, with the Jiangsu Key Laboratory of Power Transmission and Distribution Equipment Technology, Hohai University, Nanjing 210098, China, and also with the College of IoT Engineering, Hohai University, Changzhou 213022, China (e-mail: jtfei@yahoo.com).

S. Hou is with the Jiangsu Key Laboratory of Power Transmission and Distribution Equipment Technology, Hohai University, Nanjing 210098, China, and also with the College of IoT Engineering, Hohai University, Changzhou 213022, China.

Color versions of one or more of the figures in this paper are available online at http://ieeexplore.ieee.org.

Digital Object Identifier 10.1109/TNNLS.2019.2919676

systems based on a feedback linearization and multilayered feedforward neural approach. He *et al.* [12] proposed an adaptive neural tracking controller to approximate the dead-zone function and the unknown model of a robotic manipulator. A prescribed performance adaptive NN controller was investigated for a class of unknown chaotic systems in the presence of input saturation and external disturbances in [13]. Lu *et al.* [14] designed an adaptive NN controller of uncertain n-joint robotic systems with time-varying state constraints, in which an NN approximator was employed to approximate the uncertain parametric and unknown functions in a robotic system. An adaptive NN control method was investigated to stabilize a class of uncertain nonlinear strict-feedback systems with full-state constraints in [15]. An adaptive fractional order sliding-mode controller with a neural estimator was presented for a class of systems with nonlinear disturbances in [16]. Pan *et al.* [17] developed a simple adaptive NN with a proportional derivative control strategy to achieve fast and low-frequency adaptation for a class of uncertain nonlinear systems. Chen *et al.* [18] designed a globally stable direct adaptive backstepping neural tracking controller for a class of uncertain strict-feedback systems under the assumption that the accuracy of the ultimate tracking error was given *a priori*. Song *et al.* [19] developed a novel model for constructing deep NN using a fast inference predictive coding method. Liu *et al.* [20] studied an adaptive neural tracking control method for a class of uncertain nonlinear strict-feedback systems with time-varying full-state constraints.

Faced with the poor dynamic property of the feedforward NN, recurrent neural network (RNN), which is composed of feedforward neural and feedback loops, can acquire more system information. By means of superior nonlinear adaptation and learning ability of RNN, the parameters in RNN can be adjusted simply compared with the conventional NN controller. Recurrent neural structure with feedback connections naturally involves dynamic elements in the form of storing dynamic response of the system through tapped delays [21]–[29]. For instance, a novel RNN-based vector control method was suggested for a single-phase inverter with an LCL filter to approximate optimal control in [21]. Li *et al.* [22] showed a novel RNN to resolve the redundancy of manipulators for efficient kinematic control in the presence of noises in a polynomial type. An adaptive sliding-mode control system using a double-loop RNN structure was proposed for a class of nonlinear dynamic systems in [23]. Pan and Wang [24] proposed a model predictive control approach for unknown nonlinear dynamical systems based on two RNNs. An indirect intelligent sliding-mode control system utilizing a pair of hysteretic RNNs to achieve hysteresis compensation was constructed in [25]. An adaptive dynamic sliding-mode control system with an RNN for an indirect motor drive was proposed by El-Sousy [26]. Jon *et al.* [27] studied an adaptive robust control scheme based on the recurrent Elman NN to achieve high-performance speed tracking despite the system uncertainties for a sensorless permanent magnet synchronous motor servo drive. Davide and Francesco [28] discussed a simple idea that dropout regularization can be used to efficiently induce resiliency to missing inputs at prediction time by a genetic RNN. Tanaka *et al.* [29] considered two approaches to find spatially arranged sparse RNNs with the high cost-performance ratio for energy-efficient associative memory.

In practice, it is hard for the normal NN with a single hidden layer to approximate some quite complex functions. In addition, the shallow network may need a considerable number of neurons which will lead to a serious problem of computational complexity, long training time, and high memory consumption, while there are far less parameters in the deep network which can also obtain satisfactory control precision. As a consequence, a deep NN with multilayered perceptrons is designed to obtain stronger function fitting capacity and high learning accuracy [30]–[33]. It was reported in [30] that an artificial NN, in the form of a hybrid double hidden layer perceptron, can be used to provide the best prediction performance in the classification of unknown odorants into their respective chemical class. Ahmadi and Akbarizadeh [31] developed a novel human iris recognition approach based on a multilayer perceptron NN and particle swarm optimization algorithms to train the network in order to increase generalization performance. Makondo *et al.* [32] explored the feasibility of using a multilayer perceptron NN as an exploratory test oracle. A method based on the combination of decision tree algorithm and multilayer perceptron NN was proposed to identify attacks with high accuracy and reliability in [33].

Usually, it is a lack of theoretical guidance and adaptive adjustment mechanism to set up base width and central vector of Gaussian function when faced with different input signals, which requires multiple debugging manually. Motivated from the above multilayer perceptron and RNN, a double hidden layer recurrent neural network (DHLRNN)-based adaptive global sliding-mode controller with stable, robust, effective, and competitive algorithms is presented for dynamic systems. The novel DHLRNN structure could combine the advantages of deep NN and feedback NN, thereby achieving better approximation performance. In a word, the major contributions comparing with the existing ones can be summarized as follows.

1) Faced with the unknown system uncertainties and external disturbances, a novel RNN with two hidden layers is given to estimate the system nonlinearities. As the hidden layer in the NN consists of activation functions which play a significant role in making the network have the strong fitting ability, the NN with double hidden layers could realize more complex function fitting and higher training precision by fast convergence. Each node and weight has its meaning and represents a special part in the network. Moreover, recombination of activation functions gives the practical significance of the multilayered perception NN which not only could make the network more powerful to learn complex data but also could represent the mapping of an arbitrary smooth nonlinear function. From a practical application point of view, the double hidden layer NN is a more expressive network than the conventional one with a single hidden layer. The common network of the single hidden layer NN (SHLNN) needs more exponentially

nodes than the deep network like the double hidden layer NN to complete approximation. Its core is: composition of functions is more effective than the linear sum of functions. It is in favor of control precision and enhancement of response speed for dynamic systems.

2) Unlike the general NN structure, in the recurrent neural structure, the neurons of the input layer can receive signals from the neurons of the output layer. It is generally known that RNNs with feedback loops are adept at accepting past memory elements, that is, more information will be transmitted to the output node and the system can achieve better approximation performance and superior dynamic capability compared with the conventional feedforward NNs. Furthermore, the six adaptive parameters including two central vectors, two base widths, weight, and feedback gain all could adjust themselves to the optimal values adaptively, demonstrating that the system possesses more stable internal state and better approximation property in contrast with the pure NNs without feedback loops.
3) As it is difficult to establish an accurate mathematical model for dynamic systems because of their nonlinearity and uncertainties, a global sliding-mode controller based on a DHLRNN which has the salient merit of model-free control with great potential is designed to track the trajectory for a class of dynamic systems. The proposed global sliding-mode controller can ensure the global robustness especially in the approaching modal status which also accelerates the system response. The parameters of DHLRNN system regulate themselves online to the optimum stable values based on the Lyapunov adaptive laws.

This paper is organized as follows. In Section II, problem statement and an ideal global sliding-mode controller are given. Section III explains the DHLRNN, and Section IV investigates the design and stability analysis of the DHLRNN-based global sliding-mode controller. Section V shows the case study for an APF, where simulation and experimental results and some comparisons are presented. Concluding remarks are outlined in Section VI.

II. Problem Statement

Considering a class of universal multi-input systems

$$\dot{X} = AX + BU \tag{1}$$

where $X \in R^N$ denotes a state vector, $U \in R^N$ denotes a control input vector, and $A \in R^{N\times N}$ and $B \in R^{N\times N}$ are parameter matrices.

Since parameter perturbation and external disturbance exist in practice, the universal multi-input nonlinear system is described as follows:

$$\dot{X} = (A + \Delta A)X + (B + \Delta B)U + d \tag{2}$$

where ΔA and ΔB are the uncertainties of A and B, and d is an external disturbance.

The system model (1) could be rewritten as follows:

$$\dot{X} = AX + BU + F \tag{3}$$

where $F \in R^N$ is an uncertainty term, which includes parameter perturbation and external disturbance, expressed as follows:

$$F = \Delta AX + \Delta BU + d. \tag{4}$$

Assumption 1: The uncertainty F is bounded such that $\|F\| \le F_E$, where F_E is a known positive constant.

The tracking control problem is to find a control law so that the state trajectory X can track a reference trajectory X_d asymptotically. Assuming that all the system parameters are well known, the design of an ideal sliding-mode controller for nonlinear systems is described subsequently.

A tracking error is defined as follows:

$$e = X - X_d. \tag{5}$$

Then, the derivative of the tracking error is

$$\dot{e} = \dot{X} - \dot{X}_d. \tag{6}$$

Design a global sliding surface as follows:

$$S = Ce - f_0(t) \tag{7}$$

where $C \in R^{N\times N}$ is a nonsingular coefficient matrix, and $f_0(t)$ is a function specially designed for reaching the global sliding surface, satisfying the following three conditions:

1) $f_0(0) = \dot{e}_0 + Ce_0$,
2) if $t \to \infty$, $f_0(t) \to 0$,
3) $f_0(t)$ has a first derivative

where e_0 is an initial value of the tracking error.

Hence, we can design $f_0(t)$ as follows:

$$f_0(t) = f_0(0)\mathrm{e}^{-k_0 t} \tag{8}$$

where k_0 is a positive constant.

The time derivative of the global sliding surface $\dot{S}$ is

$$\begin{aligned}\dot{S} &= C\dot{e} - \dot{f}_0(t)\\ &= C(X - X_d) - \dot{f}_0(t)\\ &= C(AX + BU + F - \dot{X}_d) - \dot{f}_0(t).\end{aligned} \tag{9}$$

Making $\dot{S} = 0$, then solve the equivalent controller as follows:

$$U_{\mathrm{eq}} = (CB)^{-1}[\dot{f}_0(t) - CAX - CF + C\dot{X}_d]. \tag{10}$$

Based on the equivalent controller (10), a new controller is proposed as follows:

$$U = (CB)^{-1}[\dot{f}_0(t) - CAX + C\dot{X}_d - K\ \mathrm{sgn}(S)] \tag{11}$$

where $U_{\mathrm{sw}} = (CB)^{-1} \cdot K\mathrm{sgn}(S)$ is a switching controller, in which the sliding gain K is a designed positive constant. If all the system parameters are well known, the ideal global sliding-mode controller can be obtained as in (11).

Choose a Lyapunov function as follows:

$$V_1 = \frac{1}{2}S^T S \tag{12}$$

and its time derivative is

$$\dot{V}_1 = S^T[C(AX + BU + F - \dot{X}_d) - \dot{f}_0(t)]. \tag{13}$$

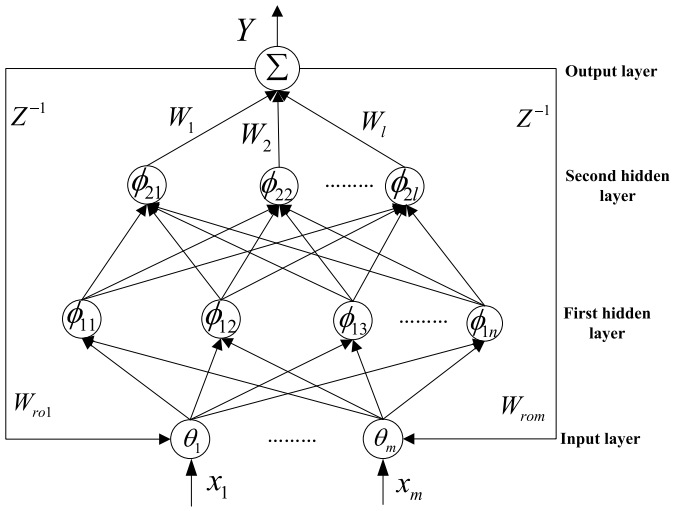

Fig. 1. Structure of DHLRNN.

Substituting the controller (11) into (13) and assuming CF is uniformly bounded as: $\|CF\| \leq F_C$, F_C is a positive constant, and it can be obtained that

$$\begin{aligned}\dot{V}_1 &= S^T[C(AX + C^{-1}(\dot{f}_0(t) - CAX + C\dot{X}_d - K\ \mathrm{sgn}(S)) \\ &\quad + F - \dot{X}_d) - \dot{f}_0(t)] \\ &= S^T[CF - K\ \mathrm{sgn}(S)] = -K\|S\| + S^T CF \\ &\leq -K\|S\| + \|S\|F_C = \|S\|(F_C - K). \end{aligned} \tag{14}$$

The above inequality (14) meets $\dot{V}_1 < 0$ when $K > F_C$. The negative definite of $\dot{V}_1$ means that V_1 and S both are bounded. From (9), we can conclude that $\dot{S}$ is also bounded; the global sliding-mode controller makes the system obtain a perfect trajectory property, and the global asymptotic stability of the closed-loop control system can be guaranteed.

However, the parameter matrix A in the control force (11) is unknown, and the ideal controller cannot be realized. Therefore, a global sliding-mode controller using a new double hidden layer feedback NN is designed to settle this problem in Sections III and IV.

III. Structure of Double Hidden Layer Recurrent Neural Network

The DHLRNN constructed by a multilayer perceptron has two hidden layers and a dynamic recurrent connection which stands for memory elements. Each node and weight has its meaning and represents a special part in the network. The adaptive parameter learning and structure learning of this new DHLRNN make this algorithm faster and more accurate than the conventional ones.

The DHLRNN is a four-layer network embedded two hidden perceptrons and an outer feedback connection. To give a clear understanding of the DHLRNN, the functional structure of each layer is depicted in Fig. 1. The first layer is an input layer composed of signal receiving nodes. However, unlike the general NN structure, the neurons of the input layer can receive signals which come back from the neurons of the output layer in the neural structure. The second layer is the first hidden layer whose neurons are mainly to accomplish the calculation of the activation functions. The main role of the activation functions is to change the linear relationship of data and accomplish nonlinear transformation, solving the problem of insufficient expression and poor classification ability of the linear model. Simultaneously, the number of neurons can be adjusted according to different situations. The third layer is the second hidden layer that ulteriorly calculates the Gaussian functions. The fourth layer is an output layer, which completes the output calculation of the novel NN for different inputs. The output signal will be propagated back to the input layer neurons through the outer feedback loop after finishing the computation of output signal in the current round. The detailed explanations of the four layers are described in the following steps.

1) *The First Layer: Input Layer*:

The input layer transmits of the input signal ($X = [x_1 x_2 .. x_m]^T$) and receives the output signal (exY) of the previous step from the output layer. The output layer is connected to the input layer by the outer weight $W_{ro} = [W_{ro1}, W_{ro2}..W_{\mathrm{rom}}]$. The output signal of the input layer is $\theta = [\theta_1, \theta_2..\theta_m]^T$, where

$$\theta_i = x_i \cdot W_{roi} \cdot ex\ Y, \quad i = 1, 2, ..., m. \tag{15}$$

2) *The Second Layer: The First Hidden Layer*:

This layer mainly maps the signals from the input space to a higher dimensional hidden space, where the signal features are linearly separable and complete the calculations of Gaussian functions. Gaussian functions are introduced to the nodes in the first hidden layer as $\Phi_1 = [\phi_{11}, \phi_{12}, ..., \phi_{1n}]^T$ and the Gaussian function of the jth node is expressed as follows:

$$\phi_{1j} = e^{-net_{1j}}, net_{1j} = \sum_{i=1}^{m} \frac{\|\theta_i - c_{1j}\|^2}{b_{1j}^2}, \quad j = 1, 2, ..., n \tag{16}$$

where the central vector is $c_1 = [c_{11} c_{12} ... c_{1n}]^T$ and the base width is $b_1 = [b_{11} b_{12} ... b_{1n}]^T$.

3) *The Third Layer: The Second Hidden Layer*:

The signals are mapped from the first hidden layer to this second hidden layer; then, the Gaussian functions are calculated again. As is similar to the second layer, each node in this layer represents a Gaussian function ϕ_{2k} which can be expressed in (17) and the total Gaussian function is denoted by $\Phi_2 = [\phi_{21}, \phi_{22}, ..., \phi_{2l}]^T$

$$\phi_{2k} = e^{-net_{2k}}, net_{2k} = \sum_{i=1}^{n} \frac{\|\phi_{1j} - c_{2k}\|^2}{b_{2k}^2} \quad k = 1, 2, ..., l \tag{17}$$

where the central vector is $c_2 = [c_{21} c_{22} ... c_{2l}]^T$ and the base width is $b_2 = [b_{21} b_{22} ... b_{2l}]^T$.

4) *The Fourth Layer: Output Layer*:

Neuron in the output layer connects with each neuron in the second hidden layer via the weights $W = [W_1, W_2, ..., W_l]^T$ and the signal node of the output layer is marked as the sum of all input signals, which is written as follows:

$$Y = W \cdot \Phi_2 = W_1 \phi_{21} + W_2 \phi_{22} + ... + W_l \phi_{2l}. \tag{18}$$

The output layer neuron is connected to the input layer neurons by the weight value W_{ro} of the output layer, and the feedback signal is recorded as exY.

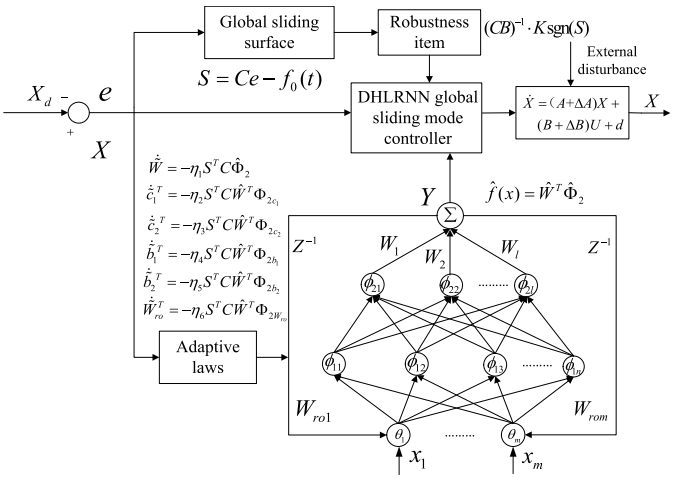

Fig. 2. Block diagram of the global sliding-mode controller using the DHLRNN controller.

IV. DHLRNN-Based Global Sliding-Mode Controller

Although the designed controller in (11) can guarantee the stability of the system, the controller could not be carried out due to the unknown matrix A. Since the DHLRNN with multicomputing layers has good ability and high precision in approximation, it can be used to approximate any complex function.

Because the function of the hidden layer is to reflect the feature mapping of the previous layer data, for an NN with only one hidden layer, the hidden layer learns the characteristics of the input data and maps the characteristics to the current hidden layer. If there is a multihidden layer NN, it is easier to realize nonlinear learning because multihidden layers could learn all the features. Moreover, based on the double hidden layer NN, the output feedback loops which reversely delivery information to input neurons are introduced, and more information will be transmitted to the output node so as to achieve better approximation effect. Therefore, the designed DHLRNN can achieve a better approximation of arbitrary smooth functions with small error, high precision, few nodes, fast convergence speed, and strong fitting ability. The block diagram of the global sliding-mode controller using the DHLRNN controller is shown in Fig. 2

Rewrite the system model (3) as follows:

$$\dot{X} = \Omega + BU + F \tag{19}$$

where $\Omega = AX$ denotes the unknown system structure which will be estimated by the DHLRNN controller.

Assumption 2: There exist optimal weight W^*, center vectors c_1^*, c_2^*, standard deviations b_1^*, b_2^*, and outer feedback gain W_{ro}^* in approximating the unknown function $\Omega = AX$ which can be expressed as $\Omega(X) = W^{*T}\Phi_2^* + \varepsilon$, where $\Phi_2^* = \Phi_2^*(X, c_1^*, c_2^*, b_1^*, b_1^*, W_{ro}^*)$, ε is the mapping error uniformly bounded as: $|\varepsilon| \le \varepsilon_b$, where ε_b is an arbitrary small positive constant.

The real output of the DHLRNN to estimate the unknown function is expressed as follows:

$$\hat{\Omega}(X) = \hat{W}^T\hat{\Phi}_2 \tag{20}$$

where $\hat{W}$ is the real estimated weight updated online and $\hat{\Phi}_2$ is the actual estimated value of the six parameters in the DHLRNN structure, expressed as follows:

$$\hat{\Phi}_2 = \hat{\Phi}_2(X, \hat{c}_1, \hat{c}_2, \hat{b}_1, \hat{b}_2, \hat{W}_{ro}).$$

Then, the error between the real value and the estimation of the unknown function Ω is derived as follows:

$$\begin{aligned}\Omega(X) - \hat{\Omega}(X) &= W^{*T}\Phi_2^* - \hat{W}^T\hat{\Phi}_2 + \varepsilon \\ &= W^{*T}(\hat{\Phi}_2 + \tilde{\Phi}_2) - \hat{W}^T\hat{\Phi}_2 + \varepsilon \\ &= W^{*T}\hat{\Phi}_2 + W^{*T}\tilde{\Phi}_2 - \hat{W}^T\hat{\Phi}_2 + \varepsilon \\ &= \tilde{W}^T\hat{\Phi}_2 + \hat{W}^T\tilde{\Phi}_2 + \tilde{W}^T\tilde{\Phi}_2 + \varepsilon \end{aligned} \tag{21}$$

where $\tilde{W}^T\tilde{\Phi}_2 + \varepsilon = \varepsilon_0$ is an approximation error.

The Taylor expansion linearization technique is employed to transform the nonlinear activation function into a partially linear form and $\tilde{\Phi}_2$ can be expressed as follows:

$$\begin{aligned}\tilde{\Phi}_2 &= \frac{\partial\Phi_2}{\partial c_1}\Big|_{c_1=\hat{c}_1}(c_1^* - \hat{c}_1) + \frac{\partial\Phi_2}{\partial c_2}\Big|_{c_2=\hat{c}_2}(c_2^* - \hat{c}_2) \\ &\quad + \frac{\partial\Phi_2}{\partial b_1}\Big|_{b_1=\hat{b}_1}(b_1^* - \hat{b}_1) + \frac{\partial\Phi_2}{\partial b_2}\Big|_{b_2=\hat{b}_2}(b_2^* - \hat{b}_2) \\ &\quad + \frac{\partial\Phi_2}{\partial W_{ro}}\Big|_{W_{ro}=\hat{W}_{ro}}(W_{ro}^* - \hat{W}_{ro}) + O_h \\ &= \Phi_{2c1}\cdot\tilde{c}_1 + \Phi_{2c2}\cdot\tilde{c}_2 + \Phi_{2b_1}\cdot\tilde{b}_1 + \Phi_{2b2}\cdot\tilde{b}_2 \\ &\quad + \Phi_{2Wro}\cdot\tilde{W}_{ro} + O_h \end{aligned} \tag{22}$$

where O_h is a high-order term, and Φ_{2c_1}, Φ_{2c_2}, Φ_{2b_1}, Φ_{2b_2}, $\Phi_{2W_{ro}}$ can be expressed in the following forms:

$$\Phi_{2c_1} = \left[\frac{\partial\Phi_{21}}{\partial c_1} \quad \frac{\partial\Phi_{22}}{\partial c_1} \quad \cdots \quad \frac{\partial\Phi_{2l}}{\partial c_1}\right]^T\Bigg|_{c_1==\hat{c}_1}$$

$$\Phi_{2c_2} = \left[\frac{\partial\Phi_{21}}{\partial c_2} \quad \frac{\partial\Phi_{22}}{\partial c_2} \quad \cdots \quad \frac{\partial\Phi_{2l}}{\partial c_2}\right]^T\Bigg|_{c_2==\hat{c}_2}$$

$$\Phi_{2b_1} = \left[\frac{\partial\Phi_{21}}{\partial b_1} \quad \frac{\partial\Phi_{22}}{\partial b_1} \quad \cdots \quad \frac{\partial\Phi_{2l}}{\partial b_1}\right]^T\Bigg|_{b_1==\hat{b}_1}$$

$$\Phi_{2b_2} = \left[\frac{\partial\Phi_{21}}{\partial b_2} \quad \frac{\partial\Phi_{22}}{\partial b_2} \quad \cdots \quad \frac{\partial\Phi_{2l}}{\partial b_2}\right]^T\Bigg|_{b_2==\hat{b}_2}$$

$$\Phi_{2W_{ro}} = \left[\frac{\partial\Phi_{21}}{\partial W_{ro}} \quad \frac{\partial\Phi_{22}}{\partial W_{ro}} \quad \cdots \quad \frac{\partial\Phi_{2l}}{\partial W_{ro}}\right]^T\Bigg|_{W_{ro}=\hat{W}_{ro}}.$$

With the proposed DHLRNN controller, according to (11), a new comprehensive controller with the DHLRNN estimator is designed as follows:

$$U = (CB)^{-1}[\dot{f}_0(t) - C\hat{\Omega} + C\dot{X}_d - K\ \mathrm{sgn}(S)]. \tag{23}$$

Consider a Lyapunov function candidate as follows:

$$\begin{aligned}V_2 &= \frac{1}{2}S^TS + \frac{1}{2\eta_1}\mathrm{tr}(\tilde{W}^T\tilde{W}) + \frac{1}{2\eta_2}\mathrm{tr}(\tilde{c}_1^T\tilde{c}_1) + \frac{1}{2\eta_3}\mathrm{tr}(\tilde{c}_2^T\tilde{c}_2) \\ &\quad + \frac{1}{2\eta_4}\mathrm{tr}(\tilde{b}_1^T\tilde{b}_1) + \frac{1}{2\eta_5}\mathrm{tr}(\tilde{b}_2^T\tilde{b}_2) + \frac{1}{2\eta_6}\mathrm{tr}(\tilde{W}_{ro}^T\tilde{W}_{ro}). \end{aligned} \tag{24}$$

Denote

$$\begin{aligned}&\frac{1}{2\eta_1}\mathrm{tr}(\tilde{W}^T\tilde{W}) + \frac{1}{2\eta_2}\mathrm{tr}(\tilde{c}_1^T\tilde{c}_1) + \frac{1}{2\eta_3}\mathrm{tr}(\tilde{c}_2^T\tilde{c}_2) \\ &\quad + \frac{1}{2\eta_4}\mathrm{tr}(\tilde{b}_1^T\tilde{b}_1) + \frac{1}{2\eta_5}\mathrm{tr}(\tilde{b}_2^T\tilde{b}_2) + \frac{1}{2\eta_6}\mathrm{tr}(\tilde{W}_{ro}^T\tilde{W}_{ro})\end{aligned}$$

as M for simplicity.

Taking the derivative of V_2, then substituting the controller (23) into the derivative of V_2 gives

$$\begin{aligned}\dot{V}_2 &= S^T\dot{S} + \dot{M}\\ &= S^T[C(AX+BU+F-\dot{X}_d)-\dot{f}_0(t)]+\dot{M}\\ &= S^T[C(AX+C^{-1}(\dot{f}_0(t)-C\hat{\Omega}+C\dot{X}_d-K\ \mathrm{sgn}(S))\\ &\quad +F-\dot{X}_d)-\dot{f}_0(t)]+\dot{M}\\ &= S^T[C\Omega - C\hat{\Omega}+CF-K\ \mathrm{sgn}(S)]+\dot{M}\\ &= S^T[C(\tilde{W}^T\hat{\Phi}_2+\hat{W}^T\tilde{\Phi}_2+\varepsilon_0)+CF-K\ \mathrm{sgn}(S)]+\dot{M}.\end{aligned} \tag{25}$$

Then, substituting the Taylor expansion (22) into (25) obtains

$$\begin{aligned}\dot{V}_2 &= S^TC\tilde{W}^T\hat{\Phi}_2 + S^TC\hat{W}^T(\Phi_{2c_1}\tilde{c}_1+\Phi_{2c_2}\cdot\tilde{c}_2+\Phi_{2b_1}\tilde{b}_1\\ &\quad +\Phi_{2b_2}\tilde{b}_2+\Phi_{2W_{ro}}\cdot\tilde{W}_{ro}+O_h)+S^TC\varepsilon_0+S^TCF\\ &\quad -KS^T\mathrm{sgn}(S)+\frac{1}{\eta_1}\mathrm{tr}(\tilde{W}^T\dot{\tilde{W}})+\frac{1}{\eta_2}\mathrm{tr}(\dot{\tilde{c}}_1^T\tilde{c}_1)+\frac{1}{\eta_3}\mathrm{tr}(\dot{\tilde{c}}_2^T\tilde{c}_2)\\ &\quad +\frac{1}{\eta_4}\mathrm{tr}(\dot{\tilde{b}}_1^T\tilde{b}_1)+\frac{1}{\eta_5}\mathrm{tr}(\dot{\tilde{b}}_2^T\tilde{b}_2)+\frac{1}{\eta_6}\mathrm{tr}(\dot{\tilde{W}}_{ro}^T\tilde{W}_{ro}).\end{aligned} \tag{26}$$

Set $S^TC\tilde{W}^T\hat{\Phi}_2+(1)/(\eta_1)\mathrm{tr}(\tilde{W}^T\dot{\tilde{W}})=0$ yields

$$\dot{\tilde{W}} = -\eta_1 S^TC\hat{\Phi}_2. \tag{27}$$

Set $S^TC\hat{W}^T\Phi_{2c_1}\tilde{c}_1+(1)/(\eta_2)\mathrm{tr}(\dot{\tilde{c}}_1^T\tilde{c}_1)=0$ yields

$$\dot{\tilde{c}}_1^T = -\eta_2 S^TC\hat{W}^T\Phi_{2c_1}. \tag{28}$$

Set $S^TC\hat{W}^T\Phi_{2c_2}\tilde{c}_2+(1)/(\eta_3)tr(\dot{\tilde{c}}_2^T\tilde{c}_2)=0$ yields

$$\dot{\tilde{c}}_2^T = -\eta_3 S^TC\hat{W}^T\Phi_{2c_2}. \tag{29}$$

Set $S^TC\hat{W}^T\Phi_{2b_1}\tilde{b}_1+(1)/(\eta_4)\mathrm{tr}(\dot{\tilde{b}}_1^T\tilde{b}_1)=0$ yields

$$\dot{\tilde{b}}_1^T = -\eta_4 S^TC\hat{W}^T\Phi_{2b_1}. \tag{30}$$

Set $S^TC\hat{W}^T\Phi_{2b_2}\tilde{b}_2+(1)/(\eta_5)\mathrm{tr}(\dot{\tilde{b}}_2^T\tilde{b}_2)=0$ yields

$$\dot{\tilde{b}}_2^T = -\eta_5 S^TC\hat{W}^T\Phi_{2b_2} \tag{31}$$

Set $S^TC\hat{W}^T\Phi_{2W_{ro}}\tilde{W}_{ro}+(1)/(\eta_6)\mathrm{tr}(\dot{\tilde{W}}_{ro}^T\tilde{W}_{ro})=0$ yields

$$\dot{\tilde{W}}_{ro}^T = -\eta_6 S^TC\hat{W}^T\Phi_{2W_{ro}}. \tag{32}$$

Substituting the adaptive laws (27)–(32) into (26) and assuming $C\varepsilon_0$, CO_{ho} are uniformly bounded as: $\|C\varepsilon_0\|\le\varepsilon_E$, $\|CO_{ho}\|\le O_E$ lead to

$$\begin{aligned}\dot{V}_2 &= S^T[CF+C\varepsilon_0+CO_{ho}]-KS^T\cdot\mathrm{sgn}(S)\\ &= S^T(CF+C\varepsilon_0+CO_{ho})-K\|S\|\\ &\le \|S\|(F_C+\varepsilon_E+O_E-K)\end{aligned} \tag{33}$$

where ε_E and O_E are positive constants.

If $K>F_C+\varepsilon_E+O_E$, then $\dot{V}_2<0$. The negative definite of $\dot{V}_2$ ensures that V_2, S are all bounded. It can be concluded that $\dot{S}$ is also bounded. The inequality $\dot{V}_2\le\|S\|(F_C+\varepsilon_E+O_E-K)$ implies that S is integrable as $\int_0^t\|S\|dt \le (1)/(F_C+\varepsilon_E+O_E-K)[V(t)-V(0)]$. Since $V(0)$ is bounded and $V(t)$ is nonincreasing and bounded, $\lim_{t\to\infty}\int_0^t\|S\|dt$ is bounded. Since $\lim_{t\to\infty}\int_0^t\|S\|dt$ is bounded and $\dot{S}$ is also bounded, according to Barbalat's lemma, $S(t)$ will asymptotically converge to 0, $\lim_{t\to\infty}S(t)=0$. Thus, the designed controller can guarantee the globally asymptotic stability of the closed-loop control system.

TABLE I
SYSTEM PARAMETERS

Supply voltage and frequency	$V_{s1}=V_{s2}=V_{s3}=220V, f=50Hz$
Three-phase diode rectifiers parameters	$R=5\,\Omega$, $L=10mH$
Single-phase diode rectifiers parameters	$R=40\,\Omega$, $L=10mH$
Active power filter parameters	$L_c=10mH$, $R_c=0.1\Omega$, $C=100\mu F$, $v_{dcref}=1000V$
Switching frequency	$f_{sw}=10KHz$

V. Simulation and Experimental Study for Active Power Filter

An illustrative example is constructed to study the performance of the global sliding-mode controller using the DHLRNN controller through a three-phase APF dynamic model [6]. The three-phase APF model is given in the following form:

$$\dot{X} = (A+\Delta A)X+(B+\Delta B)U+d \tag{34}$$

where $X=[i_1i_2i_3]^T$, $A=\mathrm{diag}\{-(R_{c1})/(L_{c1}),-(R_{c1})/(L_{c1}),-(R_{c1})/(L_{c1})\}$, $B=-(V_{\mathrm{dc}})/(L_{c1})$, $U=[u_1u_2u_3]^T$, ΔA and ΔB are the uncertainty of A and B, and d is an external disturbance.

In the proposed controller, we choose the coefficient of the sliding surface as $C=\mathrm{diag}\{1300,1300,1300\}$, the adaptive parameters as $\eta_1=0.012$, $\eta_2=0.12$, $\eta_3=0.1$, $\eta_4=0.1$, $\eta_5=0.2$, the sliding gain as $K=500$, and the parameter of the global function as $k=100$. Table I shows the system parameters utilized in the simulation.

Fig. 3 shows the curve of load current i_L, the curve of source current i_s, the tracking trajectory, and the tracking error of a compensation current i_c (select one phase current to analyze) in Fig. 3(a)–(d), respectively. From the load current in Fig. 3(a), it is apparent that distortion is very serious which is harmful to the power grid. Source current in Fig. 3(b) is well compensated after applying APF with the proposed controller at the time of 0.04 s to purify harmonic pollution effectively, where it is almost close to a smooth and sinusoidal wave. Moreover, the tracking trajectory and the tracking error of the compensation current can be observed in Fig. 3(c) and (d), in which both of them are in a wonderful state, indicating good stability and robustness.

Total harmonic distortion (THD) using the designed novel DHLRNN-based global sliding-mode controller is depicted

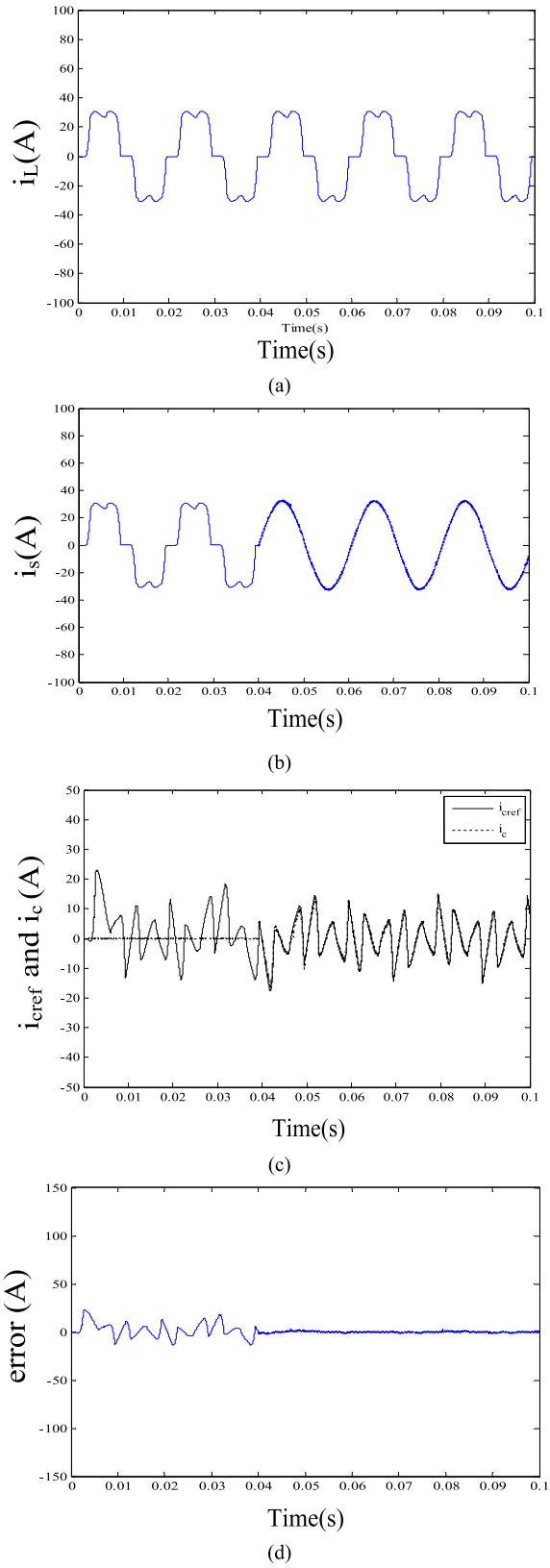

Fig. 3. Steady-state responses using the proposed controller. (a) Curve of load current. (b) Curve of source current. (c) Tracking trajectory of compensation current. (d) Tracking error of compensation current.

in Table II. THD at 0.06 s is 1.82% after APF with the proposed controller is applied to work while the one without APF is relatively extremely high (24.72%). From the above

TABLE II
COMPARISONS OF THDS

Method	WITHOUT APF	DHLRNN	SHLRNN	SHLNN
THDs	24.72%	1.82%	2.06%	2.40%

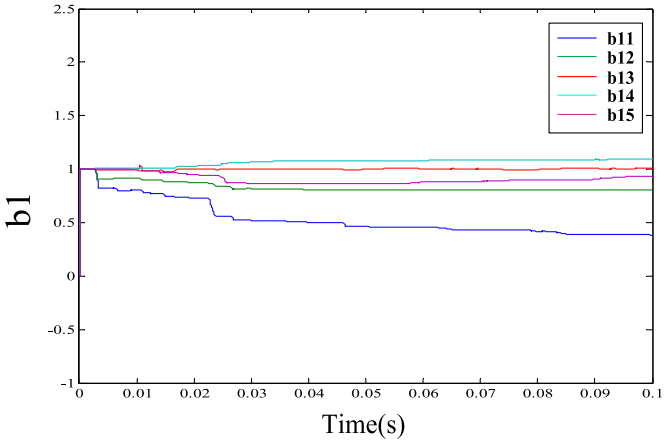

Fig. 4. Adaptation of the width b_1 of DHLRNN.

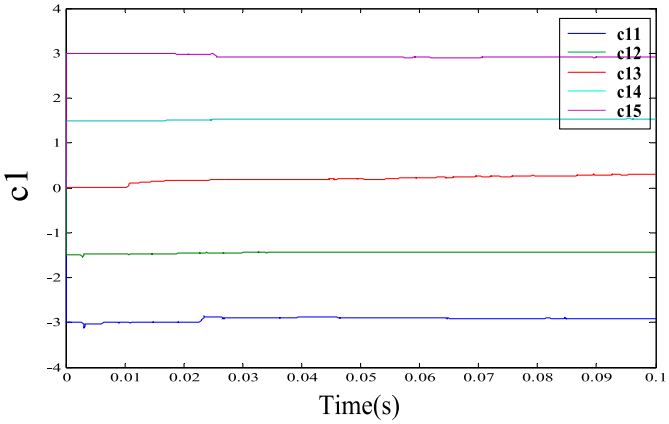

Fig. 5. Adaptation of the center c_1 of DHLRNN.

results, it is clear that the proposed control scheme is quite efficient to control the APF system in the presence of external disturbances and parameter uncertainties.

Figs. 4–9 display the adaptive curves of the six parameters in the DHLRNN controller. All these parameters containing two base widths b_1, b_2, two center vectors c_1, c_2, the network weight W, and the feedback gain W_{ro} are updated online by the adaptive laws in the Lyapunov sense and tuned transitorily to their optimal values stably. The fact that system responses can achieve satisfactory results demonstrates the strong robustness and superior self-adjusting ability of the novel DHLRNN controller.

Even with few neurons and parameters of two hidden layers, the system still can achieve efficient compensation and

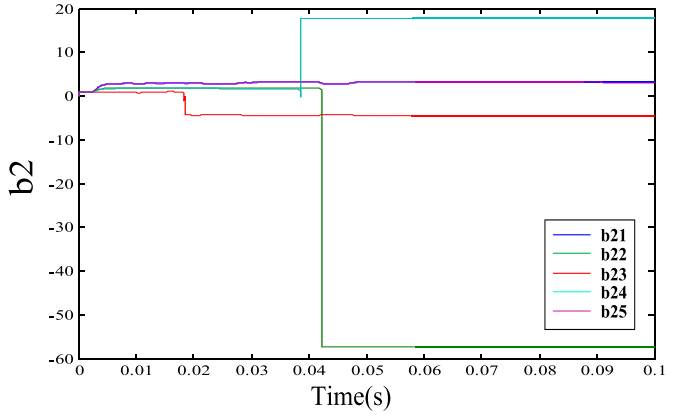

Fig. 6. Adaptation of the width b_2 of DHLRNN.

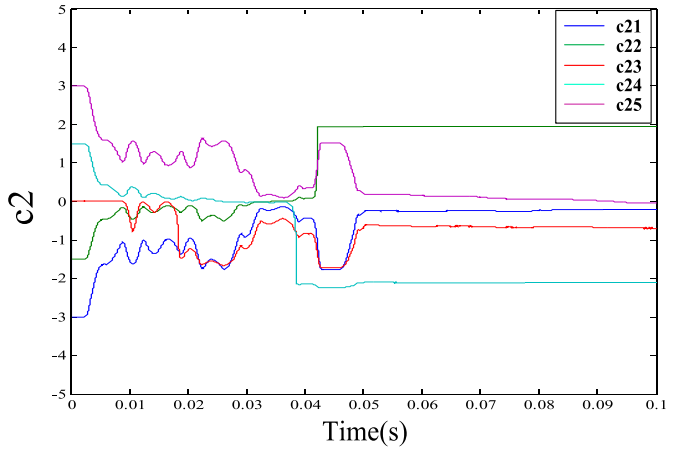

Fig. 7. Adaptation of the center c_2 of DHLRNN.

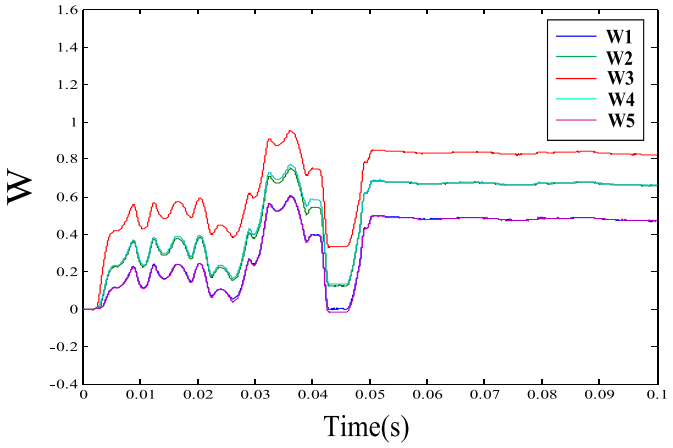

Fig. 8. Adaptation of the weight W of DHLRNN.

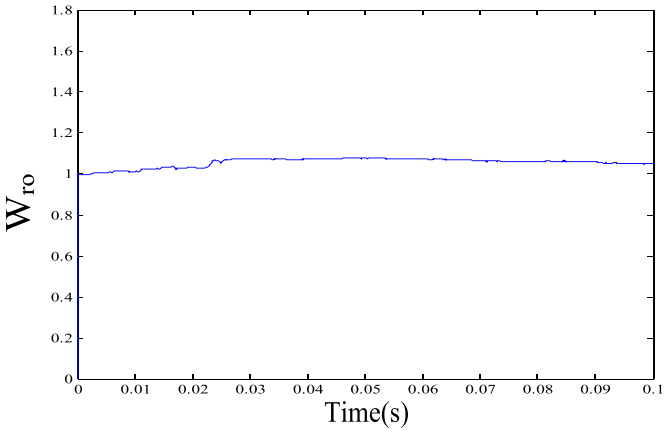

Fig. 9. Adaptation of the outer feedback W_{ro} of DHLRNN.

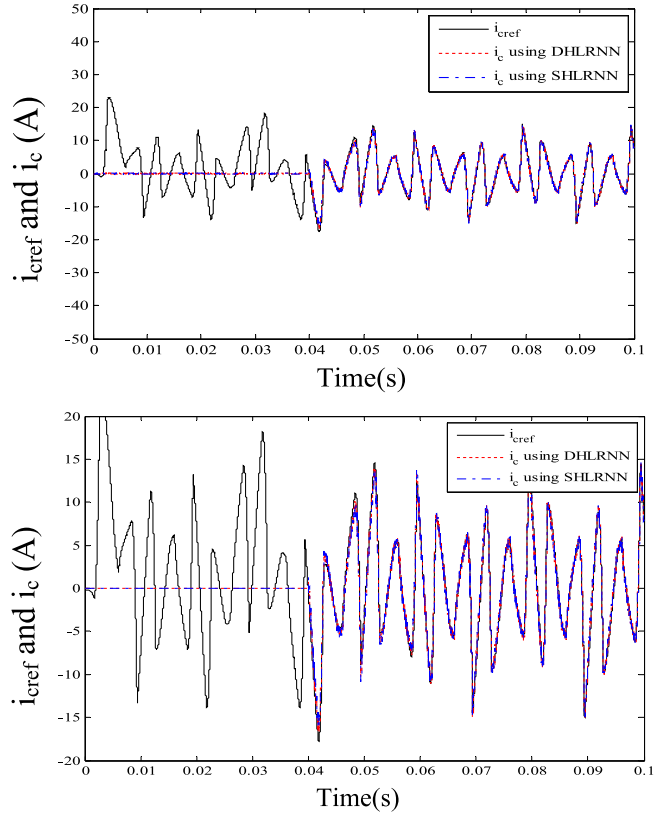

Fig. 10. Tracking trajectories comparison of compensation currents (DHLRNN–SHLRNN).

tracking effect, showing that the RNN with the double hidden layer can reduce network complexity without sacrificing precision, decrease the required adjustment parameters greatly, and speed up network training, showing great computational advantages in approximating the complex functions.

To verify the performance of the proposed DHLRNN controller more convincingly, we make three suits of comparative experiments. To make the comparisons be fair, we choose 15 nodes in the single hidden layer recurrent neural network (SHLRNN) and SHLNN and ten neurons in the DHLRNN. Figs. 10 and 11 show the comparisons of the tracking trajectories and the tracking errors of the compensation currents controlled by the DHLRNN and SHLRNN, respectively. The second pictures are the enlarged views of the first ones in both Figs. 10 and 11. As can be seen from Figs. 10 and 11, the DHLRNN (red dashed line) has smoother tracking performance and smaller tracking error than the SHLRNN (blue point line). Furthermore, the inner state of the whole system is more stable and has less dramatic changes by the DHLRNN. Compared to the DHLRNN, THD under the SHLRNN (2.06%) in Table II is a little higher which indicates the good ability to eliminate harmonics using

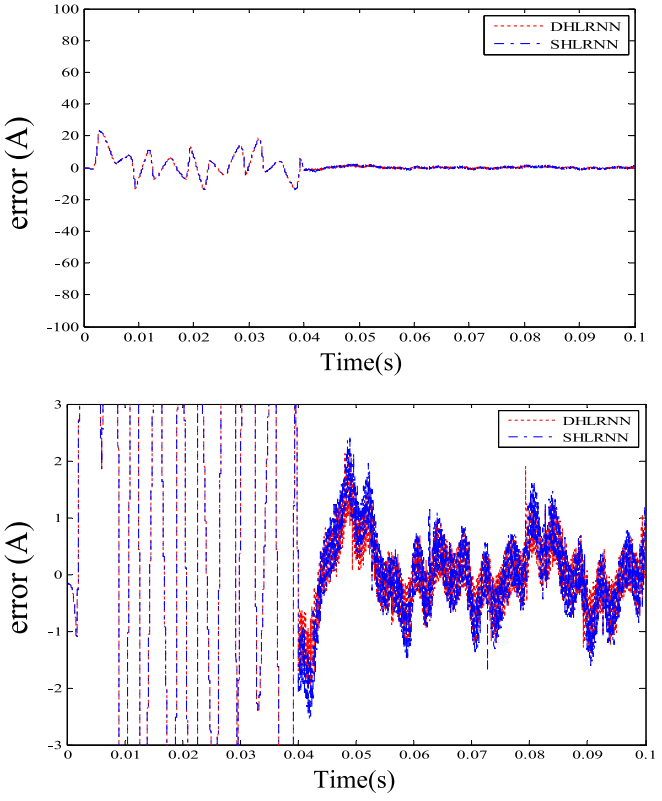

Fig. 11. Tracking errors comparison of compensation currents (DHLRNN–SHLRNN).

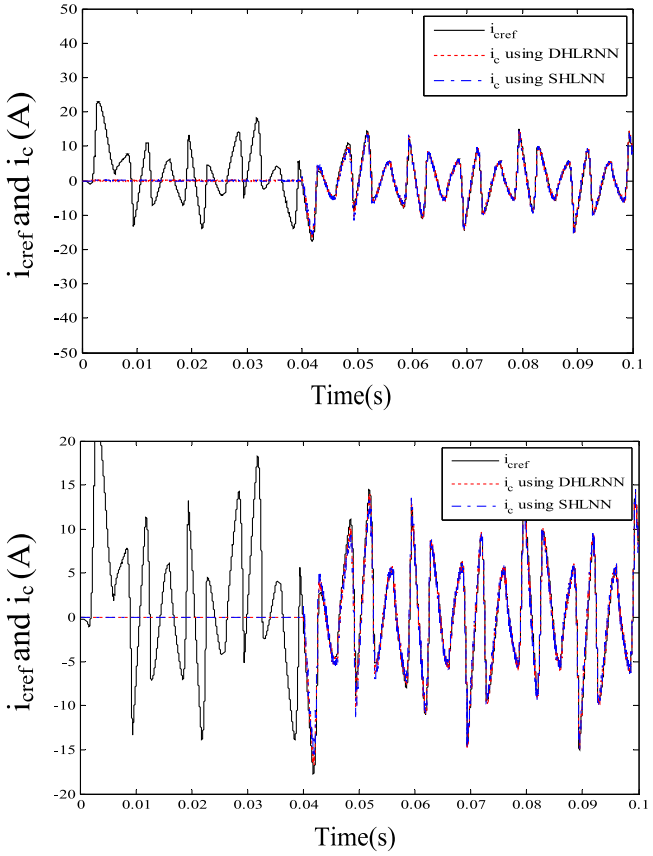

Fig. 12. Tracking trajectories comparison of compensation currents (DHLRNN–SHLNN).

the DHLRNN controller. It is concluded that the DHLRNN-based adaptive global sliding-mode controller has stronger function fitting ability, higher approximation precision, and generalization ability than the SHLRNN controller.

Similar to Figs. 10 and 11, Figs. 12 and 13 show the comparative tracking curves and tracking errors between the DHLRNN and SHLNN, respectively. The second picture is the enlarged view of the first one in each plot. It is obvious that fluctuation of the tracking trajectory in the conventional single hidden layer NN is much larger than that in the DHLRNN, and so is the tracking error meanwhile. As a result, the control capability of the presented DHLRNN is more stable and superior than the SHLNN. THD in Table II of the general NN is 2.40%, showing the performance of the SHLNN in eliminating harmonics is worse than that of the DHLRNN and the SHLRNN. It is further shown that the DHLRNN estimator can store more information, and has more expressive ability and higher accuracy of function approximation due to the addition of regression loop and second hidden layer that other methods.

Figs. 14 and 15 show the comparative tracking curves and tracking errors between the DHLRNN and proportional integral derivative global sliding mode control using the radial basis function neural network (PIDGSMCNN). From Fig. 14, it can be clearly seen that the compensation current tracks to the reference current under the DHLRNN in red quite faster than that under the PIDGSMCNN in blue, indicating the rapid response of the designed scheme. Meanwhile, the tracking accuracy is higher by the DHLRNN with a smaller error in Fig. 15. The THD under the PIDGSMCNN is 2.12% which has a weaker ability to suppress harmonic than the novel DHLRNN strategy.

To evaluate the effectiveness of the developed strategy in different cases, an unbalanced load is conducted on the APF via connecting a single-phase rectifier bridge between phase "1" and phase "2," followed by an inductor $L = 10$mH in series with a resistor $R = 40\Omega$. Fig. 16 shows the relevant curves. One could be realized that the source current is still compensated as a stable sine wave rapidly even if the load current is unbalanced.

Table II shows the comparisons of THDs. From which, it can be seen that the THD is 24.72% before using APF in controlling the system. After making the four approaches play roles in compensating the harmonics, the THD reduces to 1.82%, 2.06%, 2.12%, and 2.4%, respectively. Among these four schemes, the proposed novel DHLRNN structure possesses the best performance, indicating the superiority of the DHLRNN.

The corresponding comparisons of root-mean-square errors (RMSEs) about the four methods are summarized in Table III, showing that the DHLRNN has the smallest RMSE, and then SHLRNN, PIDGSMCNN, and SHLNN have the largest one. It is indicated that the proposed DHLRNN-based global sliding-mode controller indeed yields superior control property

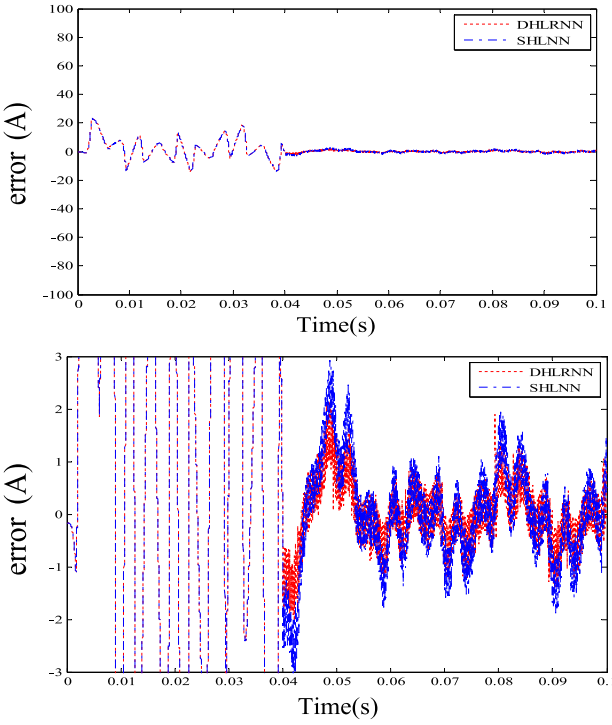

Fig. 13. Tracking errors comparison of compensation currents (DHLRNN–SHLNN).

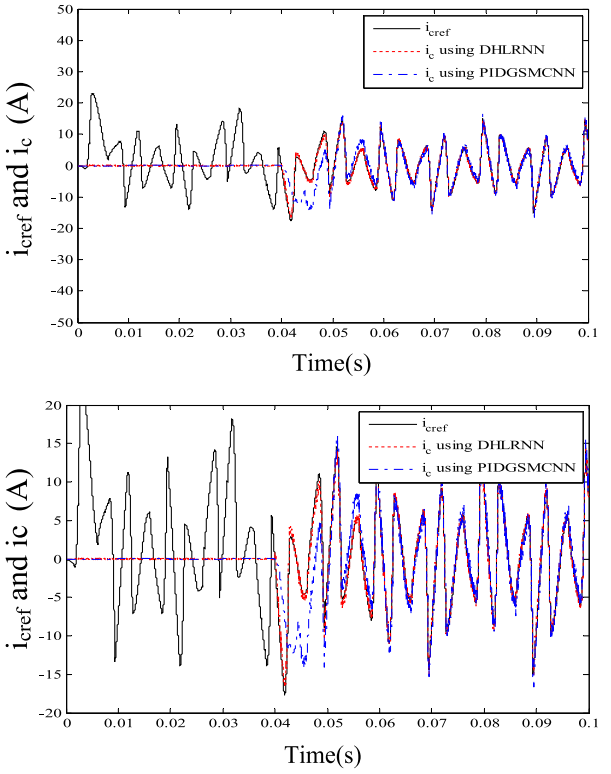

Fig. 14. Tracking trajectories comparison of compensation currents (DHLRNN–PIDGSMCNN).

than the other three methods. Moreover, the computation time is also listed in Table II using a DELL computer by the processor of Intel Xeon W-2145 CPU at 3.70 GHz with

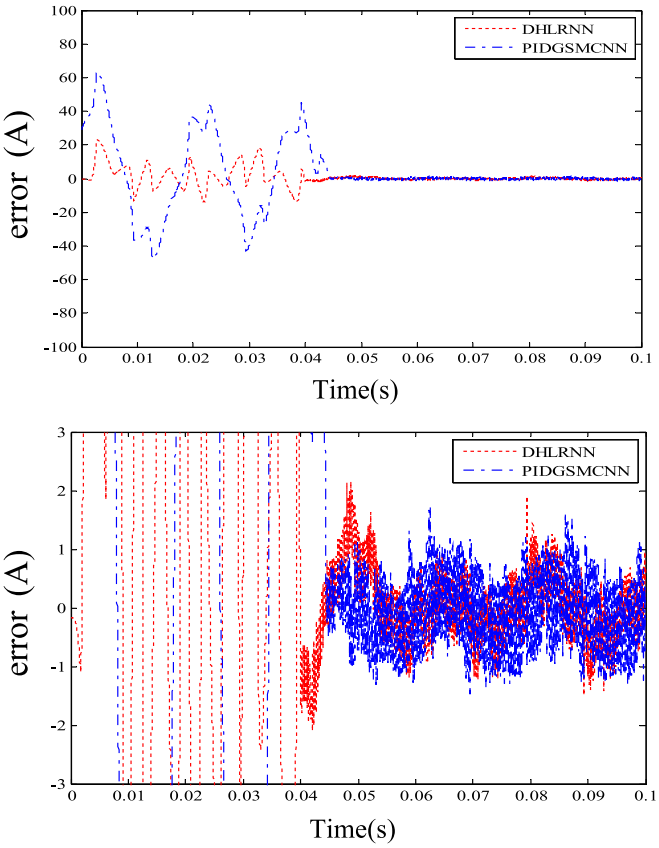

Fig. 15. Tracking errors comparison of compensation currents (DHLRNN–PIDGSMCNN).

TABLE III
COMPARISONS OF RMSES AND COMPUTATION TIME

Methods	DHLRNN	SHLRNN	PIDGSMCNN	SHLNN
RMSE	0.4566	0.6155	0.6352	0.6771
TIME(s)	147.6	135.3	79.6	41.8

the RAM of 64.0 GB. Although the computation time is extended with the increased complexity of the algorithms by the composition of Gaussian functions, the computational burden of the DHLRNN is still relatively small to obtain more satisfactory performance with fewer neurons. Thus, the novel DHLRNN structure can be widely applied in practice.

The experimental validation of the proposed control scheme for APF is implemented on the single-phase prototype, as shown in Fig. 17.

Figs. 18 and 19 show the experimental response and spectrum analysis under the DHLRNN. The waveforms in Fig. 18 are the power supply voltage, load current, compensation current, and source current, respectively. It can be apparently seen that the source current is sinusoidal, proving the effective property of the control algorithm. Through spectrum analysis in Fig. 19, the THD value of the source current is reduced to 3.42% after putting the

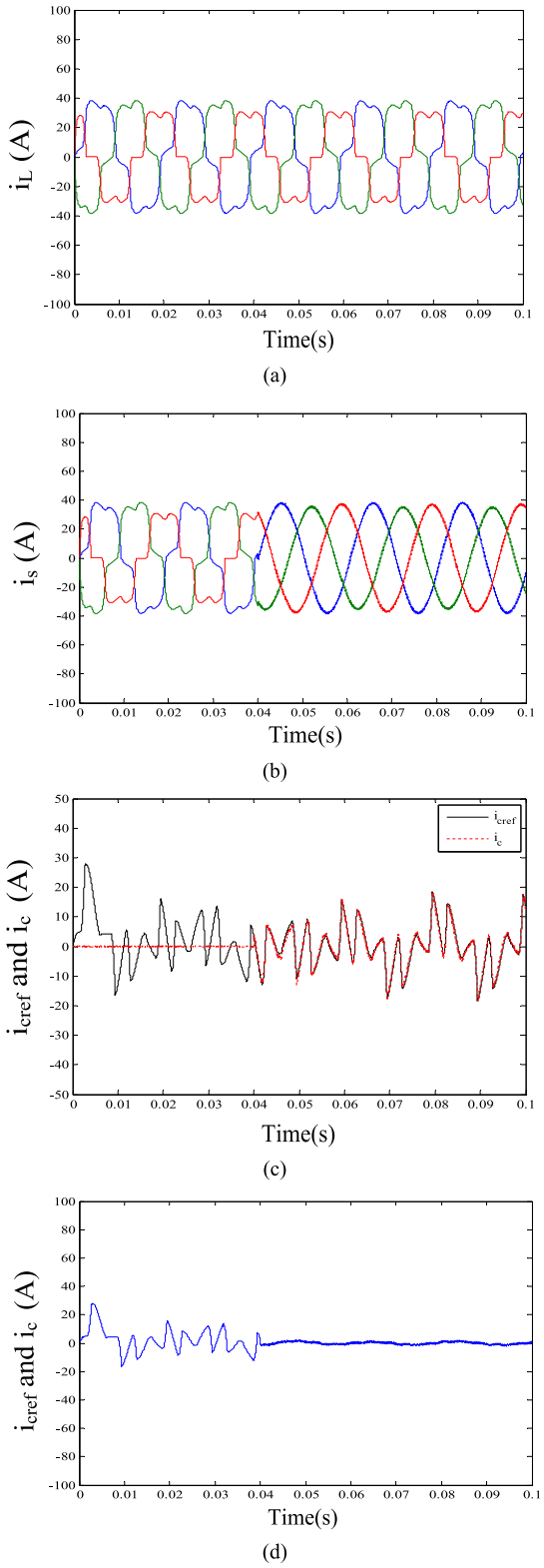

Fig. 16. System responses under the unbalanced load. (a) Load currents of three phases. (b) Source currents of three phases. (c) Tracking trajectory of compensation current. (d) Tracking error of compensation current.

APF into operation, achieving the harmonic compensation well.

In order to ulteriorly verify the superior property of the designed DHLRNN scheme, the SHLRNN method is

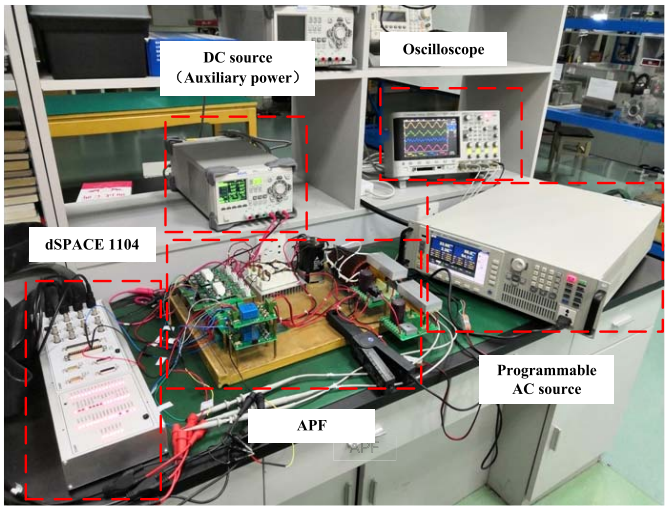

Fig. 17. Structure of the experimental prototype developed in the laboratory.

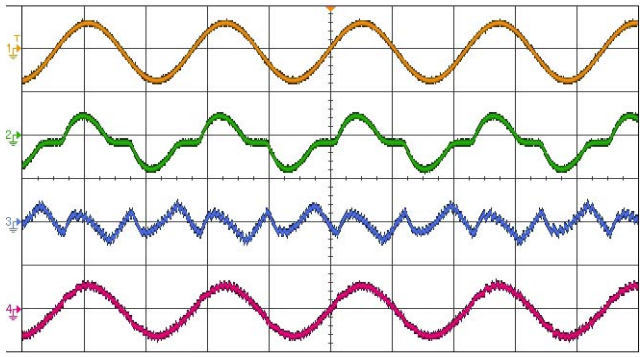

Fig. 18. Steady-state experimental results under the DHLRNN. Source voltage, load current, compensation current, and source current (from top to bottom).

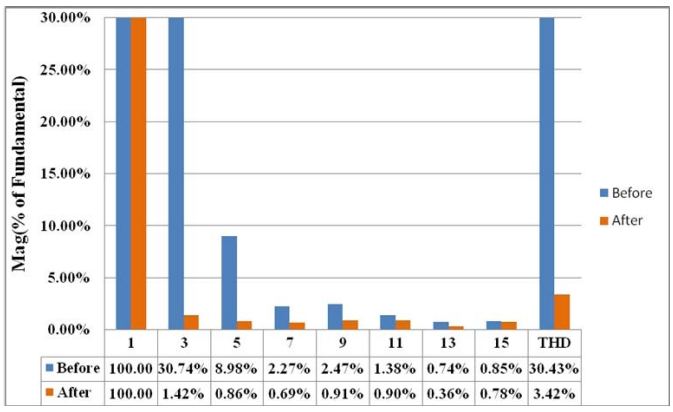

	1	3	5	7	9	11	13	15	THD
Before	100.00	30.74%	8.98%	2.27%	2.47%	1.38%	0.74%	0.85%	30.43%
After	100.00	1.42%	0.86%	0.69%	0.91%	0.90%	0.36%	0.78%	3.42%

Fig. 19. Harmonic spectrum of source current under the DHLRNN.

implemented to make experimental comparisons. Fig. 20 shows the system response under the GSMC based on the SHLRNN. It can be seen from Fig. 21 that its THD is 5.24%, which is 1.82% higher than 3.42% under the control of the DHLRNN in Fig. 19, confirming prior control effects of the proposed DHLRNN controller.

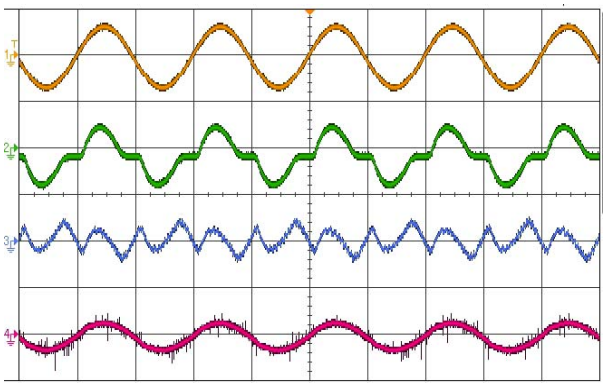

Fig. 20. Steady-state experimental results under the SHLRNN. Source voltage, load current, compensation current, and source current (from top to bottom).

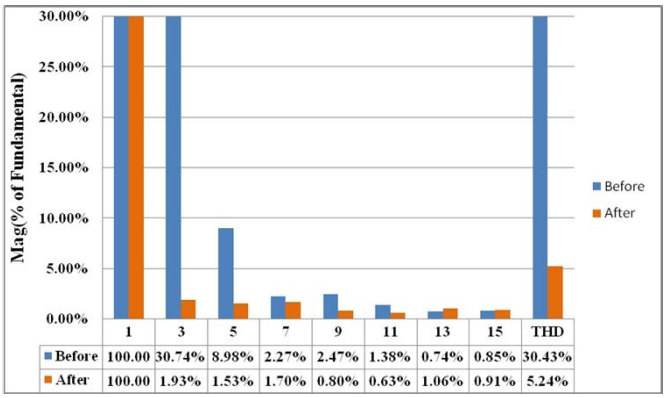

	1	3	5	7	9	11	13	15	THD
Before	100.00	30.74%	8.98%	2.27%	2.47%	1.38%	0.74%	0.85%	30.43%
After	100.00	1.93%	1.53%	1.70%	0.80%	0.63%	1.06%	0.91%	5.24%

Fig. 21. Harmonic spectrum of source current under the SHLRNN.

VI. Conclusion

A novel DHLRNN-based global sliding-mode controller is presented in this work to settle the trajectory tracking problem of multi-input universal dynamic systems with external disturbances and system uncertainties. The GSMC can overcome the shortcomings of the common sliding-mode control, making the overall system response have global robustness. Considering the approximation accuracy to complex functions, a novel double hidden layer structure is designed to realize the merits of high precision, fast speed, strong generalization ability, and efficient training regardless of requiring few neurons and parameters. For another, to improve the dynamic property of the network, an output feedback loop is added on the basis of the double hidden layer NN to approximate the unknown function well by storing more network information. The new DHLRNN is adept at accepting past memory elements, that is, more information will be transmitted to the output node and the system. In addition, six parameters containing two base widths, two center vectors, network weight, and feedback gain all could be stabilized to optimal values adaptively by the Lyapunov-based adaptive algorithm. The simulations and experiments on the APF demonstrate that the DHLRNN has the comparatively smallest scale of hidden neurons and highest accuracy among the double and single hidden layer NN schemes, showing the wonderful static and dynamic properties of the proposed novel NN structure.

Acknowledgment

The authors would like to thank the anonymous reviewers for their useful comments that improved the quality of this paper.

References

[1] H. Zhang, Q. Qu, G. Xiao, and Y. Cui, "Optimal guaranteed cost sliding mode control for constrained-input nonlinear systems with matched and unmatched disturbances," *IEEE Trans. Neural Netw. Learn. Syst.*, vol. 29, no. 6, pp. 2112–2126, Jun. 2018.

[2] M. Kühne, R. G. Rochín, R. S. Cos, G. J. R. Astorga, and A. Peer, "Modeling and two-Input sliding mode control of rotary traveling wave ultrasonic motors," *IEEE Trans. Ind. Electron.*, vol. 65, no. 9, pp. 7149–7159, Sep. 2018.

[3] M. Ghahderijani, M. Castilla, M. Castilla, A. Momeneh, J. Miret, and L. G. de Vicuña, "Robust and fast sliding-mode control for a DC–DC current-source parallel-resonant converter," *IET Power Electron.*, vol. 11, no. 2, pp. 262–271, Feb. 2018.

[4] Z. Song, C. Duan, H. Su, and J. Hu, "Full-order sliding mode control for finite-time attitude tracking of rigid spacecraft," *IET Control Theory Appl.*, vol. 12, no. 8, pp. 1086–1094, May 2018.

[5] L. Xiong, J. Wang, X. Mi, and M. W. Khan, "Fractional order sliding mode based direct power control of grid-connected DFIG," *IEEE Trans. Power Systems.*, vol. 33, no. 3, pp. 3087–3096, May 2017.

[6] Y. Chu, J. Fei, and S. Hou, "Dynamic global proportional integral derivative sliding mode control using radial basis function neural compensator for three-phase active power filter," *Trans. Inst. Meas. Control*, vol. 40, no. 12, pp. 3549–3559, Aug. 2018.

[7] D. Efimov and L. Fridman, "Global sliding-mode observer with adjusted gains for locally Lipschitz systems," *Automatica*, vol. 47, no. 3, pp. 565–570, 2011.

[8] Z. Hu, W. Hu, Z. Wang, Y. Mao, and C. Hei, "Global sliding mode control based on a hyperbolic tangent function for matrix rectifier," *J. Power Electron.*, vol. 17, no. 4, pp. 991–1003, 2017.

[9] L. Liu, Z. Han, and W. Li, "Global sliding mode control and application in chaotic systems," *Nonlinear Dyn.*, vol. 56, nos. 1–2, pp. 193–198, 2009.

[10] S. Mobayen and D. Baleanu, "Linear matrix inequalities design approach for robust stabilization of uncertain nonlinear systems with perturbation based on optimally-tuned global sliding mode control," *J. Vibrat. control*, vol. 23, no. 8, pp. 1285–1295, May 2017.

[11] T. L. Chien, C. C. Chen, Y. C. Huang, and W. J. Lin, "Stability and almost disturbance decoupling analysis of nonlinear system subject to feedback linearization and feedforward neural network controller," *IEEE Trans. Neural Netw.*, vol. 19, no. 7, pp. 1220–1230, Jul. 2008.

[12] W. He, A. O. David, Z. Yin, and C. Sun, "Neural network control of a robotic manipulator with input deadzone and output constraint," *IEEE Trans. Syst., Man, Cybern., Syst.*, vol. 46, no. 6, pp. 759–770, Jun. 2016.

[13] S. Shao, M. Chen, and X. Yan, "Prescribed performance synchronization for uncertain chaotic systems with input saturation based on neural networks," *Neural Comput. Appl.*, vol. 29, no. 12, pp. 1349–1361, Jun. 2018.

[14] S.-M. Lu, D.-P. Li, and Y.-J. Liu, "Adaptive neural network control for uncertain time-varying state constrained robotics systems," *IEEE Trans. Syst., Man, Cybern., Syst.*, to be published.

[15] Y.-J. Liu, J. Li, S. Tong, and C. L. P. Chen, "Neural network control-based adaptive learning design for nonlinear systems with full-state constraints," *IEEE Trans. Neural Netw. Learn. Syst.*, vol. 27, no. 7, pp. 1562–1571, Jul. 2016.

[16] J. Fei and C. Lu, "Adaptive fractional order sliding mode controller with neural estimator," *J. Franklin Inst.*, vol. 355, no. 5, pp. 2369–2391, 2018.

[17] Y. Pan, Q. Gao, and H. Yu, "Fast and low-frequency adaptation in neural network control," *IET Control Theory Appl.*, vol. 8, no. 17, pp. 2062–2069, Nov. 2014.

[18] W. Chen, S. S. Ge, J. Wu, and M. Gong, "Globally stable adaptive backstepping neural network control for uncertain strict-feedback systems with tracking accuracy known a priori," *IEEE Trans. Neural Netw. Learn. Syst.*, vol. 26, no. 9, pp. 1842–1854, Sep. 2015.

[19] Z. Song, J. Zhang, G. Shi, and J. Liu, "Fast inference predictive coding: A novel model for constructing deep neural networks," *IEEE Trans. Neural Netw. Learn. Syst.*, vol. 30, no. 4, pp. 1150–1165, Apr. 2019.

[20] Y.-J. Liu, L. Ma, L. Liu, S. Tong, and C. L. P. Chen, "Adaptive neural network learning controller design for a class of nonlinear systems with time-varying state constraints," *IEEE Trans. Neural Netw. Learn. Syst.*, to be published. doi: 10.1109/TNNLS.2019.2899589.

[21] X. Fu and S. Li, "Control of single-phase grid-connected converters with LCL filters using recurrent neural network and conventional control methods," *IEEE Trans. Power Electron.*, vol. 31, no. 7, pp. 5354–5364, Jul. 2015.
[22] S. Li, H. Wang, and M. U. Rafique, "A novel recurrent neural network for manipulator control with improved noise tolerance," *IEEE Trans. Neural Netw. Learn. Syst.*, vol. 29, no. 5, pp. 1908–1918, Apr. 2017.
[23] J. Fei and C. Lu, "Adaptive sliding mode control of dynamic systems using double loop recurrent neural network structure," *IEEE Trans. Neural Netw. Learn. Syst.*, vol. 29, no. 4, pp. 1275–1286, Apr. 2018.
[24] Y. Pan and J. Wang, "Model predictive control of unknown nonlinear dynamical systems based on recurrent neural networks," *IEEE Trans. Ind. Electron.*, vol. 59, no. 8, pp. 3089–3101, Aug. 2012.
[25] J. H. Wiest and G. D. Buckner, "Indirect intelligent sliding mode control of antagonistic shape memory alloy actuators using hysteretic recurrent neural networks," *IEEE Trans. Control Syst. Technol.*, vol. 22, no. 3, pp. 921–929, May 2014.
[26] F. F. M. El-Sousy, "Adaptive dynamic sliding-mode control system using recurrent RBFN for high-performance induction motor servo drive," *IEEE Trans Ind. Informat.*, vol. 9, no. 4, pp. 1922–1936, Nov. 2013.
[27] R. Jon, Z. Wang, C. Luo, and M. Jong, "Adaptive robust speed control based on recurrent elman neural network for sensorless PMSM servo drives," *Neurocomputing*, vol. 227, pp. 131–141, Mar. 2017.
[28] D. Bacciu and F. Crecchi, "Augmenting recurrent neural networks resilience by dropout," *IEEE Trans. Neural Netw. Learn. Syst.*, to be published. doi: 10.1109/TNNLS.2019.2899744.
[29] G. Tanaka *et al.*, "Spatially arranged sparse recurrent neural networks for energy efficient associative memory," *IEEE Trans. Neural Netw. Learn. Syst.*, to be published. doi: 10.1109/TNNLS.2019.2899344.
[30] L. R. Bachtiar, C. P. Unsworth, and R. D. Newcomb, "Super E-noses: Multi-layer perceptron classification of volatile odorants from the firing rates of cross-species olfactory receptor arrays," in *Proc. 36th Annu. Int. Conf. IEEE Eng. Med. Biol. Soc.*, Chicago, IL, USA, Aug. 2014, pp. 954–957.
[31] N. Ahmadi and G. Akbarizadeh, "Hybrid robust iris recognition approach using iris image pre-processing, two-dimensional Gabor features and multi-layer perceptron neural network/PSO," *IET Biometrics*, vol. 7, no. 2, pp. 153–162, Mar. 2018.
[32] W. Makondo, R. Nallanthighal, I. Mapanga, and P. Kadebu, "Exploratory test oracle using multi-layer perceptron neural network," in *Proc. Int. Conf. Adv. Comput., Commun. Inform. (ICACCI)*, Jaipur, India, Sep. 2016, pp. 1166–1171.
[33] J. Esmaily, R. Moradinezhad, and J. Ghasemi, "Intrusion detection system based on multi-layer perceptron neural networks and decision tree," in *Proc. 7th Conf. Inf. Knowl. Technol. (IKT)*, Urmia, Iran, May 2015, pp. 1–5.

Yundi Chu received the B.S. and M.S. degrees in electrical engineering from Hohai University, Nanjing, China, in 2013 and 2016, respectively. She is currently pursuing the Ph.D. degree in electrical engineering with Hohai University.

Her current research interests include power electronics, adaptive control, intelligent control, and nonlinear control.

Juntao Fei (M'03–SM'14) received the B.S. degree in electrical engineering from the Hefei University of Technology, Hefei, China, in 1991, the M.S. degree in electrical engineering from the University of Science and Technology of China, Hefei, in 1998, and the M.S. and Ph.D. degrees in mechanical engineering from The University of Akron, Akron, OH, USA, in 2003 and 2007, respectively.

He was a Visiting Scholar with the University of Virginia, Charlottesville, VA, USA, from 2002 to 2003. He was a Post-Doctoral Research Fellow and an Assistant Professor with the University of Louisiana at Lafayette, Lafayette, LA, USA, from 2007 to 2009. He is currently a Professor with Hohai University, Nanjing, China. His current research interests include adaptive control, nonlinear control, intelligent control, dynamics and control of MEMS, and smart materials and structures.

Shixi Hou received the B.S. degree in automation from Hohai University, Nanjing, China, in 2011, and the Ph.D. degree in electrical engineering from Hohai University, in 2016.

He is currently a Lecturer with Hohai University. His current research interests include power electronics, adaptive control, nonlinear control, and intelligent control.